

Distributed Generation Interface to the CERTS Microgrid

H. Nikkhajoei, *Member, IEEE*, R. H. Lasseter, *Fellow, IEEE*

Abstract— This paper focuses on the energy storage system and the power electronic interface included in microsources of the CERTS microgrid. To provide the plug-and-play feature and the power quality requirements of the CERTS microgrid, all microsources regardless of their prime mover type must have a unified dynamic performance. This necessitates attaching an energy storage module to some or all of the microsources. The storage module is attached to the prime mover through a power electronic interface that couples the microsource to the microgrid. Details of the energy storage module, the power electronic interface and the corresponding controls are described. Performance of an example microsource, which includes a synchronous generator, a storage module and an electronic interface, is studied. Dynamic performance of the example microsource when operating in the CERTS microgrid is evaluated based on digital time-domain simulations in the EMTP-RV software environment. Effectiveness of the storage module, the electronic interface and the corresponding controls in enhancing the microsource performance is verified.

Index Terms— Microgrid, Microsource, Distributed Generation, Electronic Interface, Energy Storage, Power Quality, Dynamics.

I. INTRODUCTION

DISTRIBUTED generation is a promising concept that is considered as an alternative solution for addressing technical, economical and environmental issues of conventional power systems [1]-[3]. Distribution of generation units within an electric power system offers technical advantages in terms of power quality and reliability as well as energy management and efficiency. It also offers economical advantages in terms of reducing capital investment for construction of power systems since distribution of generation units eliminates the need for having extensive transmission systems. Distributed Generation (DG) power systems provide environmental benefits as a result of offering a more efficient way of generating and distributing electricity as well as enabling the integration of renewable energy resources [4]. As a new concept for the electric power industry, the application of DG for power systems is under extensive studies and experimental tests and there are many technical issues in terms of the operation, control and protection of DG systems [5]-[7].

An alternative solution to realize the emerging potential of DG is to view the Distributed Resources (DR) and the associated loads as a small power system that is called microgrid. The CERTS microgrid employs an advanced approach that enables integrating an unlimited number of DRs with the electricity grid, without requiring changes in the structure of existing power systems [8]. The CERTS microgrid concept is driven by the following principles: (1) a system perspective for customers, utilities and society to capture the full benefits of integrating DRs with the electricity

grid, and (2) a business motivation for accelerating adoption of the microgrid concept by reducing the corresponding initial investment and enhancing the value of microgrids [9]. The goal of developing the CERTS microgrid is to accelerate realization of small scale DG systems that offer attractive advantages such as (i) supplying waste heat to buildings, that eliminates the need for extensive thermal distribution networks, and (ii) enhancing the quality of power which is delivered to sensitive loads [6].

The CERTS microgrid requires that all of its microsources have a unified dynamic performance, regardless of their prime mover type. This insures the plug-and-play feature and the power quality performance that are expected from the CERTS microgrid. Prime movers such as internal combustion engines, gas turbines, microturbines, photovoltaics, fuel cells and wind turbines have different dynamics depending on the prime mover size and the technology used. To provide a unified dynamic performance for microsources with different prime movers, an energy storage module must be included in the microsources. A power electronic interface controls the operation of storage module based on dynamics of the prime mover. This insures that all microsources have the same load-following performance at their point of coupling with the microgrid. This paper describes the operation of CERTS microgrid, details of an energy storage module and an electronic interface for microsources, and detailed simulation of a variable-speed synchronous generator based microsource when operating in the CERTS microgrid.

II. CERTS MICROGRID

The CERTS microgrid has two critical components, the static switch and the microsource. The static switch has the ability to autonomously island the microgrid from disturbances such as faults, IEEE 1547 events and power quality events. After islanding, each microsource can seamlessly balance the power on the islanded microgrid using a power vs. frequency droop controller. The frequency droop also insures that the microgrid frequency is different from the grid to facilitate reconnection to the utility. The reconnection of microgrid to the utility grid is achieved autonomously when the tripping event is no longer present. The synchronization is carried out by using the frequency difference between the islanded microgrid and the utility grid, insuring a transient free operation without having to match frequencies and phase angles at the connection point.

The basic microgrid architecture is shown in Fig. 1. It consists of a group of radial feeders which can be a part of a distribution system or a building electrical system. There is a single point of connection to the utility that is called the point of common coupling [10]. Feeders A to C have sensitive loads

which require local generation. The microgrid of Fig. 1 has four microsources at nodes 8, 11, 16 and 22. The microsources control the microgrid operation using only local voltage and current measurements. Feeder D does not have a sensitive load and therefore, no local generation is required for this feeder. When the microgrid is grid-connected, power from the local generation can be directed to the non-sensitive loads of Feeder D.

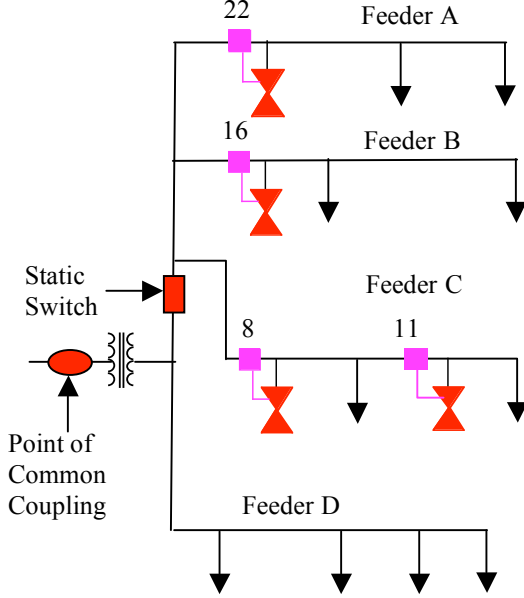


Fig. 1: CERTS microgrid.

When there is a problem with the utility supply, the static switch isolates the sensitive loads (Feeders A to C) from the utility grid in less than a cycle. Non-sensitive loads (Feeder D) ride through the event. It is assumed that the microsources provide sufficient generation which meets the power demands of Feeders A, B, and C.

The CERTS microgrid requires that the microsources have a unified dynamic performance. Microsources such as small Internal Combustion (IC) engine gensets, microturbine generators and fuel cells have different dynamics. Therefore, each microsource must have a fast-response energy storage (surge) module to minimize the impacts of microsource dynamics on the microgrid operation. The storage can be batteries or supercapacitors that are connected to the dc bus of the electronic interface of each microsource. The dc storage has several advantages over ac storages. First, the dc storage decouples dynamics of a microsource from those of the microgrid, which reduces oscillations between the microsources. Second, the dc storage provides modularity, where each microsource has the energy storage required for a fast dynamic response and is not dependent to a central ac storage system. The modularity promotes the microgrid reliability and therefore, the loss of one storage module does not significantly impact the operation of microgrid. In contrast, the loss of an ac storage system can greatly reduce the functionality of a microgrid.

III. POWER ELECTRONIC-INTERFACED MICROSOURCE

Different types of microsources that are used in a microgrid have time constants in the range of hundreds of milliseconds to tens of seconds, when responding to a power change. For instance, a small IC engine generator has a time constant of 250 ms, while a microturbine generator or a fuel cell has a time constant in the range of tens seconds. This section develops a power electronic interface that can be universally used for any type of microsource regardless of its dynamic response.

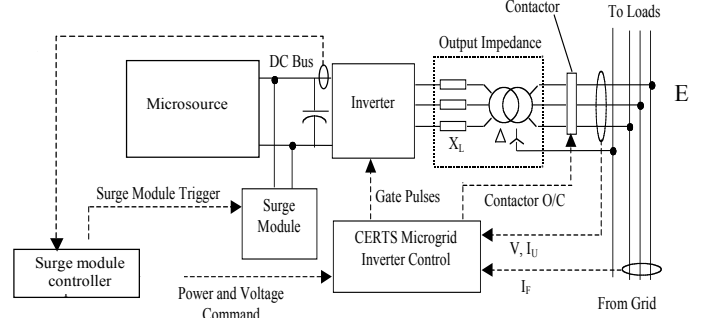


Fig. 2: A power electronic-interfaced microsource.

Fig. 2 shows a block diagram of the power electronic interface required for coupling a microsource to the CERTS microgrid. The interface includes a storage (surge) module and an inverter, and is connected to a dc voltage generated by the microsource. The inverter converts the input dc voltage to a three-phase voltage with a desired frequency, magnitude and phase angle at the output terminals. The surge module is activated during fast load changes to provide the instantaneous power difference between the load and the microsource. This insures that the load demand is provided with a high power quality. The surge module also regulates the rate of microsource power change after a load increase, insuring that the microsource does not exceed its dynamic capability. Otherwise, the microsource may stall under large load changes, which has been experienced from the CERTS microgrid field tests.

IV. INVERTER

A. Overview

Fig. 2 shows the block diagram of a microsource that is coupled to a microgrid through a voltage-sourced inverter. As a minimum, the inverter needs to control the flow of real and reactive powers between the microsource and the microgrid. Although the real and reactive powers (P, Q) are coupled, P is primarily controlled by the power angle δ while Q is regulated by the inverter terminal voltage V . Therefore, it is possible to independently control the real and reactive powers. The following equations provide relationships between P and Q and the inverter output voltage magnitude V and angle δ .

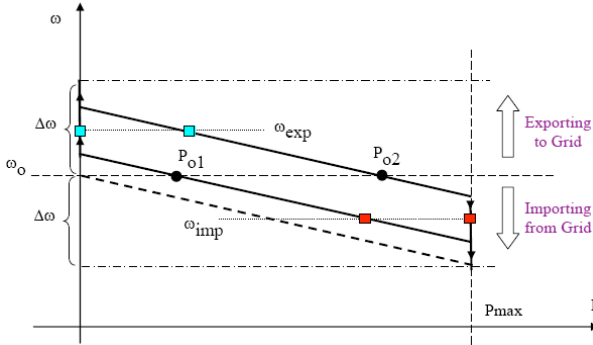
$$P = \frac{3VE}{2\omega L} \sin \delta \quad (1)$$

$$Q = \frac{3V}{2\omega L} (V - E \cos \delta) \cdot \quad (2)$$

E is the voltage magnitude at the point of common coupling. If the coupling inductance L is sized so that δ is less than 10° , then P is proportional to δ and Q is proportional to V [11]. Given the values of P and Q , V and δ are determined from the power vs. frequency and the voltage vs. reactive power droops of the microsource.

B. Power vs. Frequency Droop

Consider a grid-connected microgrid which includes two microsources. Each microsource has a constant negative slope droop on the P - ω plane [9], Fig. 3. The power set points of microsources are P_{o1} and P_{o2} which represent the amounts of



power injected by the microsources at the grid frequency of ω_o . The frequency drops by a given amount of $\Delta\omega$ as the power spans from zero to P_{max} .

Fig. 3: Power vs. frequency droop.

When the grid power is lost because of IEEE 1547 events, voltage drops, faults, blackouts and so on, the microgrid is autonomously transferred to an island operation. If the system imports power from the grid prior to islanding, then the microsources need to increase their power to balance power of the island. The new operating point will be at a frequency lower than ω_o . In the case shown in Fig. 3, both microsources increase their output power and microsource 2 reaches its maximum power at the frequency ω_{imp} . If the system exports power to the grid prior to islanding, then the new frequency will be higher than ω_o . The microsources generate less output power with microsource 1 injecting no power at the frequency ω_{exp} .

Fig. 3 shows the steady-state characteristics of microsources. The characteristics have a fixed slope in the region where the microsources operate within their power limits $(0, P_{max})$. The slope becomes vertical at the limits. Each characteristic is the locus where the steady-state points are constrained to come to rest. However, during dynamics the trajectory deviates from the characteristic. The relationship between power and frequency in the linear region of characteristic is given by

$$m = \frac{\Delta\omega}{P_{max}} \quad (3)$$

$$\omega = \omega_o - m(P - P_o) \cdot \quad (4)$$

P_o and ω_o are the microsource power and frequency when the microgrid is grid-connected, and P and ω are those of the islanded microgrid.

C. Voltage vs. Reactive Power Droop

Integration of a large number of microsources, implied in the microgrid concept, is not possible with the basic P - Q control of conventional distributed generation systems. Voltage regulation of each microsource is necessary for reliability and stability of a microgrid. Without local voltage control, microgrids with a high penetration of microsources can experience voltage and/or reactive power oscillations.

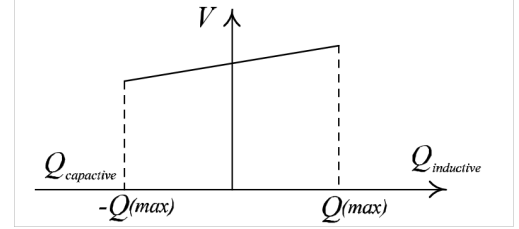


Fig. 4: Voltage vs. reactive power droop.

Unlike a large power system, the impedance between microsources in a microgrid is small. Small errors in the microsources voltage set points cause large circulating currents that can exceed ratings of the microsources. This can be prevented by a voltage vs. reactive power droop control. Fig. 4 illustrates the basic function of a controller that operates based on the voltage vs. reactive power droop. When the reactive power generated by a microsource becomes more capacitive, the microsource output voltage is reduced to control the local voltage, Fig. 4. Conversely, as the reactive power becomes more inductive, the voltage set point is increased. The reactive power limit Q_{max} is a function of the volt-ampere VA rating of the inverter and the real power of the prime mover P as follows.

$$Q_{max}^2 = (VA)^2 - P^2 \cdot \quad (5)$$

D. Control

To comply with the microgrid requirements, each microsource controller must respond autonomously to microgrid changes without requiring a communication with other microsources [9]. Fig. 5 shows the block diagram of a controller for the inverter of a microsource. The blocks on the left calculate real-time values of the inverter output real and reactive powers (P, Q) and the voltage E at the point of coupling of the microsource based on local data. The power and voltage droops are implemented in separate blocks. The controller generates required voltage magnitude V and angle δ at the inverter terminals which are given as inputs to a signal generator. The signal generator is responsible to issue correct switching signals for the power electronics inside the inverter to track the requested voltage magnitude and angle. The switching signals are generated based on the Space Vector Modulation (SVM) switching strategy.

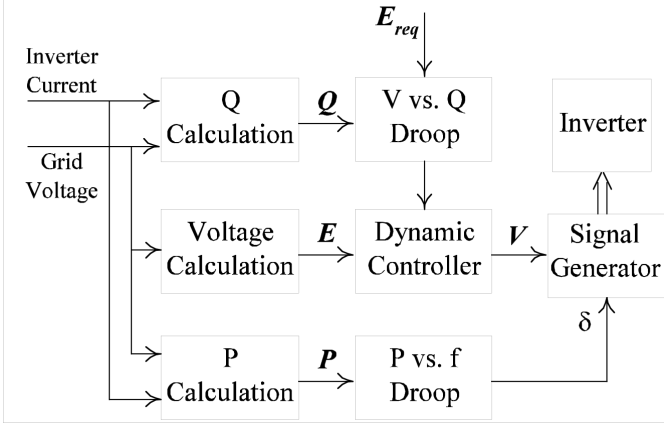


Fig. 5: Block diagram of the inverter controller.

V. SURGE MODULE

A. Principles of Operation

The surge module is a key component for proper functionality of the microsource of Fig. 2. It insures the microgrid power quality during transients, and controls rate of the microsource power increase. The ideal operation of a surge module is shown in Fig. 6. Following a load increase, the surge module provides power while the microsource increases its output power at a pre-specified rate. When the microsource output power becomes greater than the load demand, the surge module starts recharging at a controlled rate. When fully charged, the surge module moves to a standby state.

Assume that the load is suddenly increased at time t_1 , Fig 6(a). The microsource, Fig. 6(b), and the surge module, Fig. 6(c), together provide the instantaneous load power. Fig. 6(a) shows that the inverter input current i_l suddenly increases from i_{l1} to i_{l2} at $t=t_1$, in response to the load increase. Fig. 6(b) shows the microsource output current i_s as it increases from i_{l1} to i_{l2} at a pre-specified rate of $R_1=di_s/dt$. The rate of increase of i_s is regulated by the surge module controller, Fig. 2. The surge module injects the current difference between the load i_l and the source i_s , Fig. 6 (c). Fig. 6 (d) shows the energy lost by the surge module during the discharging period.

When the discharging period is completed at t_2 , the charging process begins and the microsource provides power for both the load and the surge module. Figs. 6 (a) to (c) show the load, source and surge module currents during the charging period (t_2, t_4). Magnitude of the charging current i_{sm} depends on the amount of energy that is required for a full charge of the energy storage. However, in the first charging period (t_2, t_3), i_{sm} is limited to $-I_{sm(max)}$, while in the second period (t_3, t_4), i_{sm} is proportional to the surge module energy shortage ΔE_{sm} . Fig. 6 (d) shows variation of the energy during the charging period of the surge module. At t_4 , the surge module is fully charged and moves to the standby mode.

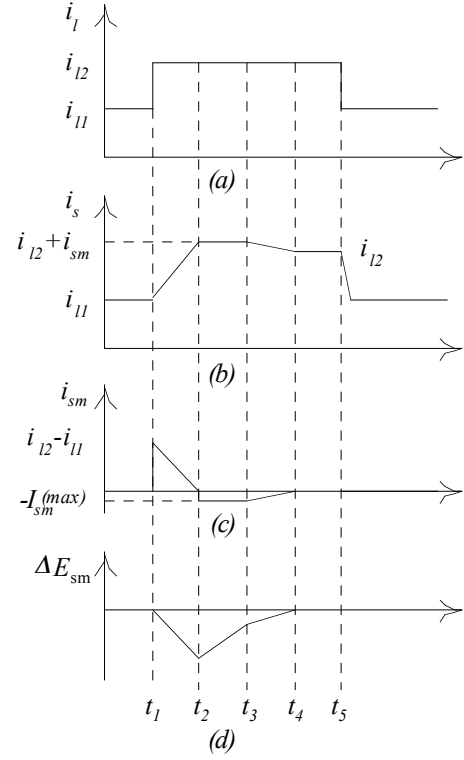


Fig. 6: Basic operation of the surge module of Fig. 2: (a) load current drawn by the inverter; (b) dc current provided by the microsource; (c) surge module current; and (d) energy difference from a fully charged state.

At t_5 , the load is reduced to its initial value, Fig. 6 (a). The current i_s is decreased at a rate $R_2=di_s/dt$ which is many times higher than that of the current increase rate R_1 , Fig. 6 (b). The rate depends on the method used by the microsource to discharge energy, e.g., breaking resistors. Ideally, the current i_s must be reduced with the same rate of the load current decrease to prevent an excessive over voltage at the interface DC-link. The surge module current i_{sm} is zero after the load current decrease unless the module is in the middle of a charging period, Fig. 6 (c).

B. Design Considerations

To design the surge module, its required energy and duty cycle of operation must be known. The amount of energy provided by the surge module during the discharging period depends on both the load change and the rate of microsource power increase. For the load increase of Fig. 6 (a), the surge module discharged energy during the period (t_1, t_2), Fig. 6 (d), is

$$\Delta E_{sm}(t_2) = \frac{v_{dc}}{2} (i_{l2} - i_{l1})(t_2 - t_1) = \frac{v_{dc}(i_{l2} - i_{l1})^2}{2R_1}, \quad (6)$$

where v_{dc} is the DC-link voltage, $R_1=(i_{l2}-i_{l1})/(t_2-t_1)$ and $\Delta E_{sm}(t_2)$ is absolute value of the energy change that is shown in Fig. 6(d).

The storage component of the surge module, whether it is a battery or a supercapacitor, must be able to provide the energy $\Delta E_{sm}(t_2)$ given by (6). The amount of energy lost by the surge module during the discharging period, (6), is equal to that of the charging period. This principle is used to estimate the time

required for a full charge of the surge module. The total charge time is sum of the periods $\Delta t_1 = t_3 - t_2$ and $\Delta t_2 = t_4 - t_3$, Fig. 6 (d). Assume that the charging current i_{sm} is proportional to the absolute value of energy shortage ΔE_{sm} , i.e., $\Delta E_{sm} = k_e i_{sm}$, where the gain k_e is equal to $-v_{dc}$. The magnitude of charging current is saturated at $I_{sm(max)}$ for the period of (t_2, t_3) . If $\Delta E_{sm}(t_2) > v_{dc} I_{sm(max)}$, the time t_3 corresponds to $\Delta E_{sm}(t_3) = v_{dc} I_{sm(max)}$. Otherwise, $\Delta t_1 = 0$ since the magnitude of i_{sm} is less than $I_{sm(max)}$ from the beginning of the charging period. Thus,

$$\Delta t_1 = \begin{cases} \frac{\Delta E_{sm}(t_2)}{v_{dc} I_{sm(max)}} - 1 & \Delta E_{sm}(t_2) > v_{dc} I_{sm(max)} \\ 0 & \text{Otherwise} \end{cases} \quad (7)$$

Assuming that the voltage v_{dc} is the same for both the discharging and the charging periods and substituting $\Delta E_{sm}(t_2)$ from (6) in (7), we obtain

$$\Delta t_1 = \begin{cases} t_{sat} - 1 & t_{sat} > 1 \\ 0 & \text{Otherwise} \end{cases} \quad (8)$$

where $t_{sat} = (i_{l2} - i_{l1})^2 / (2R_l I_{sm(max)})$ seconds. For the period of (t_3, t_4) , the current i_{sm} is proportional to the energy shortage ΔE_{sm} as indicated by the following equation.

$$i_{sm}(t) = -\frac{\Delta E_{sm}(t)}{v_{dc}} = -\frac{\Delta E_{sm}(t_3)}{v_{dc}} - \int_{t_3}^t i_{sm}(t) dt. \quad (9)$$

Taking derivative of (9) and assuming that v_{dc} is constant, we deduce

$$\frac{di_{sm}(t)}{dt} + i_{sm}(t) = 0. \quad (10)$$

Solving (10) for i_{sm} , we obtain

$$i_{sm}(t) = k_i e^{-(t-t_3)} \quad (11)$$

where

$$k_i = -\frac{\Delta E_{sm}(t_3)}{v_{dc}} \quad (12)$$

$$\Delta E_{sm}(t_3) = \begin{cases} v_{dc} I_{sm(max)} & t_{sat} > 1 \\ t_{sat} v_{dc} I_{sm(max)} & \text{Otherwise} \end{cases} \quad (13)$$

Assume that the surge module is considered to be fully charged when the charging current i_{sm} is 2 percents of $-I_{sm(max)}$. Therefore, the time of full charge t_4 corresponds to $i_{sm}(t_4) = -0.02 I_{sm(max)}$. Substituting (12) and (13) in (11) and considering the constraint $i_{sm}(t_4) = -0.02 I_{sm(max)}$, the charging period Δt_2 is obtained

$$\Delta t_2 = t_4 - t_3 = \begin{cases} 3.9 & t_{sat} > 1 \\ -\ln \frac{0.02}{t_{sat}} & 0.02 < t_{sat} \leq 1 \\ 0 & t_{sat} \leq 0.02 \end{cases} \quad (14)$$

The total charge time Δt_{ch} of the surge module from (8) and (14) is

$$\Delta t_{ch} = \Delta t_1 + \Delta t_2 = \begin{cases} t_{sat} + 2.9 & t_{sat} > 1 \\ -\ln \frac{0.02}{t_{sat}} & 0.02 < t_{sat} \leq 1 \\ 0 & t_{sat} \leq 0.02 \end{cases} \quad (15)$$

Based on (15), with the charging strategy of Fig. 6 (c), the total time required for charging the surge module is always greater than 3.9 seconds when $t_{sat} > 1$ second. Equation (15) was obtained based on the assumption that i_{sm} during the charging period varies between $-I_{sm(max)}$ and zero. If the current i_{sm} is set at the constant value of $-I_{sm(max)}$ during the entire charging period, then the total charging time Δt_{ch} is

$$\Delta t_{ch} = \frac{\Delta E_{sm}(t_2)}{v_{dc} I_{sm(max)}}. \quad (16)$$

Substituting $\Delta E_{sm}(t_2)$ from (6) in (16), we obtain

$$\Delta t_{ch} = t_{sat}. \quad (17)$$

This indicates a faster charging of the surge module, where the charging time is 2.9 seconds less than Δt_{ch} given by (15) for $t_{sat} > 1$ second.

C. Control

This section develops a control system for the surge module of Fig. 2 to operate based on the principles presented in Section V-A. Based on the operation principles, the source current i_s of the interface of Fig. 2 must increase with a pre-specified rate R_l after a load increase. The current i_s must also decrease at a greater rate R_2 when the load decreases.

Fig. 7 shows the block diagram of a control system for the surge module of Fig. 2. The part on the top of the control system that has the input i_l and the output i_s^* generates a reference signal for the current i_s^* . At steady state, $i_s^* = i_l$ and thus, the comparator output is zero and the integrator output is constant at the common value of source and load currents. When the load increases, the comparator output becomes 1 and the integrator output i_s^* increases with the rate R_l and settles at the new value of i_l . When the load decreases, the comparator output becomes -1 and the integrator output decreases with the rate R_2 and settles at the new value of i_l .

After a load increase, the surge module must accommodate the power difference between the input source and the output load of the interface. To accommodate the power difference, the control system of Fig. 7 generates a reference for the surge module current i_{sm}^* that is the difference between the load and source currents.

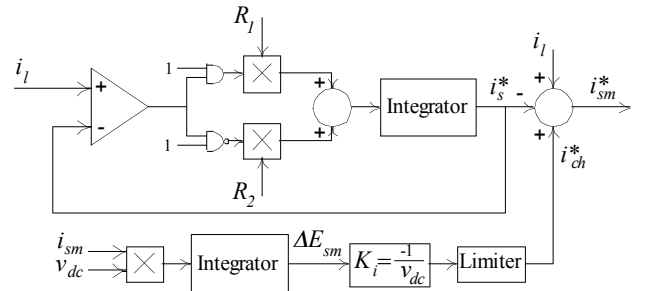


Fig. 7: The surge module controller of Fig. 2.

When the source power reaches a level that it can provide

the full load power, charging of the surge module begins. The bottom-side part of the control system of Fig. 7 generates a reference for the surge module current during the charging period. The integrator block estimates energy change ΔE_{sm} of the surge module for both the discharging and the charging periods. When the discharging is completed, ΔE_{sm} generates a negative reference current for the surge module i_{sm}^* which charges the storage. During the charging period, the current i_{sm}^* is equal to i_{ch}^* since $i_s^* = i_l$. It is also proportional to ΔE_{sm} and is limited between $-I_{sm(max)}$ and zero. The system of Fig. 7 is a simple, comprehensive controller for the surge module of Fig. 2. The controller regulates output powers of both the surge module and the microsource during all operating conditions.

D. Battery Sizing

The surge module of Fig. 2 includes an energy storage component that is coupled to the inverter through a power electronic converter. The CERTS microgrid requires the surge module to respond quickly to load/generation changes. Among existing energy storage technologies, batteries and supercapacitors are cost-effective fast-response storage systems that meet the microgrid requirements [12]. The CERTS microgrid uses battery as the energy storage system for its microsources. For each microsource, the battery is coupled through a boost DC-DC converter to the microsource inverter.

Several basic factors govern the size, including the number of cells and rated capacity, of a battery. This includes required minimum and maximum voltages and duty cycle of the battery as well as temperature and aging factors and the design margin [13]. Consider that $V_b(min)$ and $V_b(max)$ represent minimum and maximum voltage requirements of the battery for the surge module of Fig. 2. Required number of the battery cells N_c is obtained from

$$N_c = \frac{V_b(max)}{V_c}, \quad (18)$$

where V_c is the cell voltage required for a satisfactory charging which is specified by the manufacturer. When designing the battery, the required minimum cell voltage is obtained from

$$V_c(min) = \frac{V_b(min)}{N_c}. \quad (19)$$

The capacity of a battery string is the same as that of a single cell. The ampere-hour capacity of a battery cell for the surge module of Fig. 2 is obtained as follows. The battery must provide the power difference between the source generation and the load demand after a load increase. Consider that initially the source and the load powers are zero. The battery has to provide a maximum energy when the load has a step increase from zero to the rated source power P_{sr} . At the time of load increase, the battery should provide an output power equal to P_{sr} . Thus, the battery output current has a maximum magnitude of $I_b(max) = P_{sr}/V_b(min)$ at the time of load increase. The battery current decreases to zero with the rate of source current increase R_l , Fig. 6(c).

The ampere-hour capacity that is used as an initial value for sizing the battery cells is the integral of the battery current

during the discharging period (t_l, t_2), Fig. 6.

$$C_c(ini) = \frac{1}{2} \frac{(t_2 - t_l)}{3600} I_b(max) = \frac{1}{7200} \frac{P_{sr}^2}{R_l V_{dc} V_b(min)} \quad (20)$$

In (20), $t_2 - t_l = i_{sr}/R_l = P_{sr}/(R_l V_{dc})$, where i_{sr} is the rated source current. The capacity of a cell is a function of its output current. Therefore, the total cell capacity is obtained by taking the time integral of the capacities required for infinite small periods, where in each period the current is assumed to be constant. Thus, the total cell capacity required for the discharging period (t_l, t_2) is

$$C_c = \int_{t_l}^{t_2} i_b(t) k(t) dt \quad (21)$$

$i_b(t)$ is the instantaneous battery current and k is the capacity rating factor that is specified by the manufacturer for a given capacity class of $C_c(ini)$ [13]. For the surge module of Fig. 2, the battery current changes linearly during the discharge period, Fig. 6. To account for the current changes impact on the capacity, the discharging period (t_l, t_2) is divided to N equal sections. Thus, the cell capacity given by (21) can be written as

$$C_c = I_b(max) \left[\left(1 - \frac{1}{2N}\right) k_N - \frac{1}{N} \sum_{j=2}^N k_j \right], \quad (22)$$

where k_j is the capacity rating factor related to the end point of Section j . When selecting the battery size, the capacity C_c must be multiplied by the following correction factors: temperature derating factor k_T ; design margin factor k_d ; and aging factor k_a . Typical values of these factors are $k_T=(1.1, 1.25)$, $k_d=1.1$ and $k_a=1.25$ [13].

VI. EXAMPLE MICROSOURCE

This section considers an example microsource that is coupled to a microgrid through the electronic interface of Fig. 2. Study of the example microsource demonstrates performance of the interface of Fig. 2 that is controlled by the system of Fig. 7. Fig. 8 shows a schematic representation of the microsource that includes an (internal combustion) IC engine and a synchronous generator and is connected to the interface through a boost rectifier. The IC engine operates in a variable-speed mode to produce different values of output mechanical power. Since the speed is variable, the generator produces a three-phase voltage with a variable amplitude and frequency. The generator voltage is converted to a regulated dc voltage at the interface input terminals by the boost rectifier.

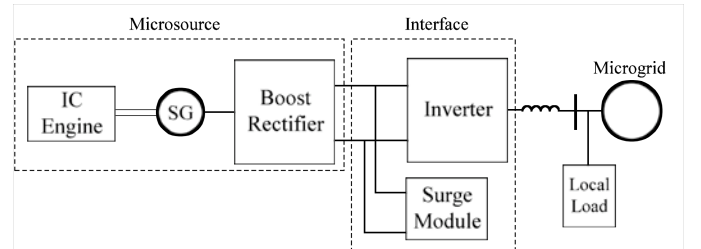


Fig. 8: An IC engine microsource coupled to a microgrid through the electronic interface of Fig. 2.

A. Internal Combustion Engine

The prime mover of the microsource of Fig. 8 is an IC

engine whose fundamentals of operation and details can be found in the technical literature [14]-[16]. A model that represents adequately an IC engine for power system studies of a diesel-powered generator is shown in Fig. 9, [15]. The model includes an actuator that determines fuel-flow rate ϕ_f from the engine throttle position θ . The main block represents the engine that has a gain K_e , an efficiency η_e , and a time delay τ_e . The engine output is the developed mechanical torque T_m that drives the generator.

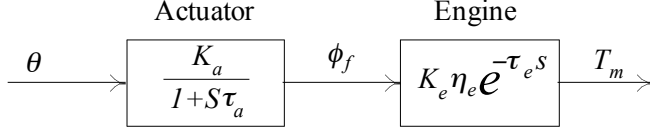


Fig. 9: A simplified representation of an IC engine.

Fig. 10 shows the horsepower versus speed of a typical IC engine for different throttle positions. The number besides each curve represents the amount of manifold vacuum in Hg, where the curve on the top corresponds to a wide open throttle position. The graph indicates that moving from point 1 to 2 the engine develops a higher mechanical power as the speed increases. For an optimal operation, speed versus horsepower of the engine must follow the curves of Fig. 10.

Fig. 11 shows the block diagram representation of a governor that controls the generator speed based on the curves of Fig. 10. A speed reference ω_{mr} is given as input to the governor and the output is the mechanical torque T_m which inputs the generator. The governor includes a controller and

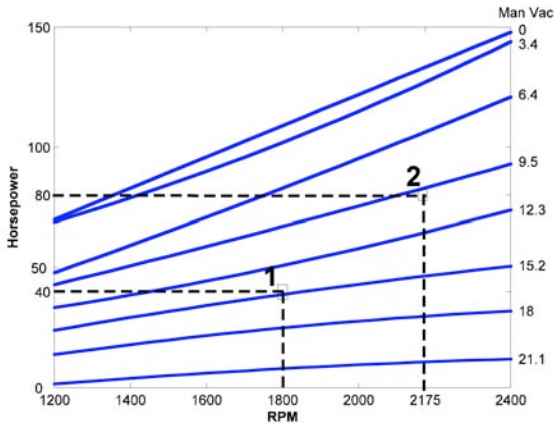


Fig. 10: Horsepower versus speed curves of an IC engine.

the engine model. The controller is a Proportional-Integral (PI) block in series with a limiter and determines fuel-flow rate ϕ_f of the engine from the speed reference and measured values. The engine model considers the engine delay and efficiency and the engine gain which is calculated from the power versus speed curves of Fig. 10. Fig. 11 shows how the engine gain is calculated from the input fuel-flow rate ϕ_f at a given speed ω_m . The fuel-flow rate is converted to an equivalent manifold vacuum. A block which represents the mechanical power versus speed curves of Fig. 10 specifies the engine horsepower for the given manifold vacuum and speed. Instantaneous value of the engine gain is calculated as the ratio of instantaneous mechanical torque and the engine fuel-

flow rate and is given as the input K_e to the governor.

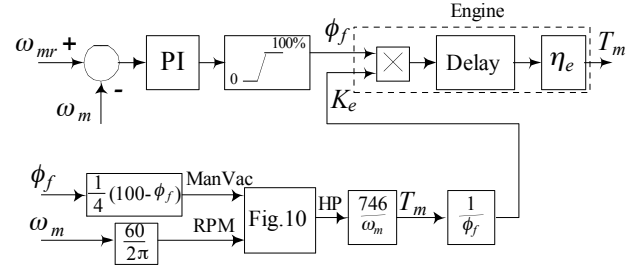


Fig. 11: The IC engine governor.

B. Synchronous Generator

The electrical generator of the microsource of Fig. 8 is a three-phase synchronous generator which converts mechanical energy of the IC engine to electrical form. Unlike conventional synchronous generators, the generator of Fig. 8 is a variable-speed machine and operates within a range of speeds with which the IC engine spins. The generator produces a three phase voltage whose amplitude and frequency are proportional to the generator speed. The generator is a 75 KVA, 480 V, 60 Hz, 4-pole synchronous machine. It has a field winding and one damper winding in the d-axis and one damper winding in the q-axis. Parameters of the generator are given in Table I.

TABLE I
PARAMETERS OF THE GENERATOR OF FIG. 8

Rated power, S	75 KVA
Nominal voltage, v_g	480 V
Nominal frequency, f_g	60 Hz
Number of poles, P	4
Armature resistance, R_a	0.029 pu
Armature leakage reactance, X_{la}	0.25 pu
Zero sequence reactance, X_0	0.034 pu
D-axis Parameters	
Reactance, X_d	1.714 pu
Transient reactance, X'_d	0.342 pu
Sub-transient reactance, X''_d	0.258 pu
Transient time constant, τ'_d	0.05 s
Sub-transient time constant, τ''_d	0.006 s
Q-axis Parameters	
Reactance, X_q	1.714 pu
Transient reactance, X'_q	0.342 pu
Transient time constant, τ'_q	0.05 s
Moment of inertia, J	0.134 Kg.m ²
Damping coefficient, D	0.013 N.s/m

C. Simulation Results

This section presents detailed simulation results of the system shown in Fig. 8. The microsource uses an IC engine that is modeled as shown in Fig. 9 with the governor of Fig. 11. The synchronous generator is modeled using EMTP-RV machine model. Parameters of the generator, the surge module controller and the IC engine are given in Table I and Table II. The power electronics of the inverter, the dc-dc converter of the surge module and the boost rectifier are modeled to the device level. The dc storage of the surge

module is modeled as an ideal dc source behind an impedance network. The inverter and the surge module are controlled by the control systems of Fig. 5 and Fig. 7. Dynamic response of the system of Fig. 8 to load changes is shown in Figs. 12-14. The system is initially operating in steady-state and delivers 30 kW power to the load. The power increases to 60 kW at $t=5$ seconds, and is reduced to 30 kW at $t=7$ seconds.

TABLE II
Surge module controller parameters, Fig. 7

R_1	140 amps/sec	K_i	-0.0012 amps/joule
R_2	2800 amps/sec		
IC engine parameters, Figs. 9 & 11			
K_a	84	τ_e	8 milliseconds
τ_a	0.3 seconds	η_e	0.625

Fig. 12 shows response of the dc bus of the system of Fig. 8 to the load changes, where the graphs are similar to those shown in Fig. 6. Fig. 12(a) shows that the current i_l demanded by the inverter has a step increase at $t=5$ seconds and a step decrease at $t=7$ seconds. Fig. 12(b) shows the effectiveness of the surge module controller in regulating the rate of power increase of the microsource. This is seen in the controlled rate of the dc current i_s provided by the microsource after the load increase. The increase rate is controlled by the constant R_1 in Fig. 7. The current i_s decreases with a larger rate R_2 . Fig. 12(c) shows the current of surge module during the load increase. This current provides the difference between the power demanded by the inverter and the power available from the microsource. After the microsource reaches its desired output, the current i_{sm} becomes negative to recharge the surge module.

Fig. 12(d), ΔE_{sm} , illustrates the discharging/charging cycle of the surge module, where $\Delta E_{sm} = 0$ indicates a fully charged state. One can compare Fig. 12(a) to (d) with the corresponding graphs of Fig. 6(a) to (d) that illustrates basics of operation of the surge module of Fig. 2. Fig. 12(e) shows the actual dc bus voltage, which was assumed to be constant in Fig. 6.

Fig. 13 shows response of the inverter of Fig. 8 at its microgrid side. Fig. 13(a) shows changes of the inverter output power and Fig. 13(b) illustrates changes of the microgrid frequency that is controlled by the inverter. The power and frequency values are coupled through the power vs. frequency droop shown in Fig. 3. The droop is designed such that a power increase of 60 kW would decrease the frequency by 0.5 Hz. This event has an approximate power increase of 30 kW resulting in a frequency decrease of approximately 0.25 Hz. Fig. 13(c) shows the step changes of the load current. Fig. 13(d) illustrates effectiveness of the inverter voltage controller of Fig. 5 that operates based on the voltage vs. reactive power droop of Fig. 4. The load has a near constant voltage magnitude with no significant variations during the transients.

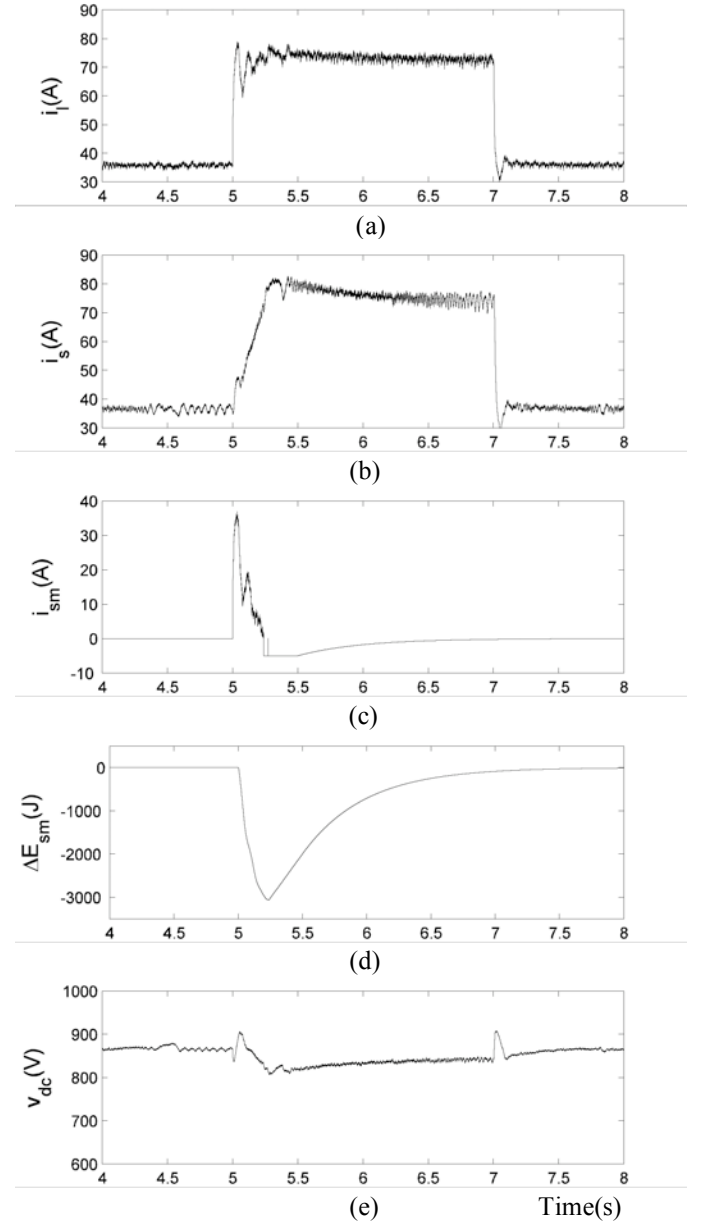


Fig. 12: Dynamic response of the dc bus of the system of Fig. 8: (a) inverter dc-side current; (b) dc current provided by the microsource; (c) surge module current; (d) energy difference from a fully charged state; and (e) dc bus voltage.

Fig. 14 shows dynamic response of the generator to the load changes. Fig. 14(a), the generator output power, and Fig. 14(b), the generator current, demonstrate effectiveness of regulating the generator power increase rate by the controller of Fig. 7, which prevents the generator stalling under large load increases. Fig. 14(c) shows variations of the generator speed that is regulated by the control system of Fig. 11. To track the optimal power vs. speed curves of Fig. 10, the speed of IC engine is increased when the load increases.

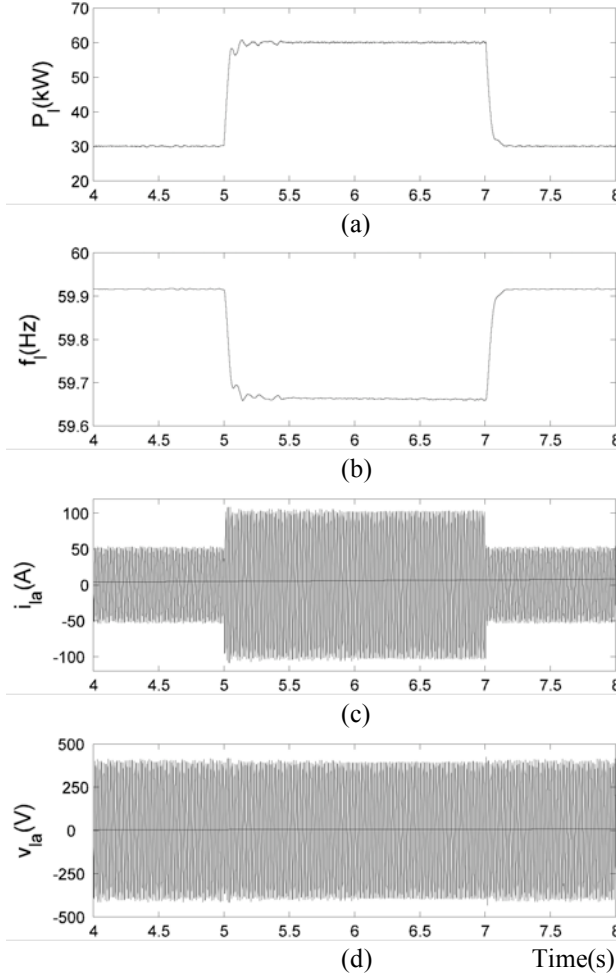


Fig. 13: Dynamic response of the inverter of Fig. 8 at its microgrid side: (a) inverter output power; (b) microgrid frequency; (c) load current; and (d) load voltage.

VII. CONCLUSIONS

This paper introduces a power electronic interface, including an energy storage (surge) module and an inverter, for coupling distributed resources (microsources) with a microgrid. A control system for the electronic interface is developed that regulates the rate of power increase of a microsource based on its dynamic capability. This prevents the generator stalling under large load increases for microsources with a synchronous generator or a microturbine generator, and accounts for the power increase delay of fuel cells. The developed control system also regulates the power that is exchanged with the surge module based on the available source power and the load demand. This provides a unified dynamic response in terms of load-following capability for microsources with any type of prime mover, and insures the plug-and-play feature and the power quality performance that are required for a microgrid.

Performance of the proposed electronic interface when coupling a variable-speed synchronous generator based microsource to the CERTS microgrid was evaluated based on simulation of the system in the EMTP-RV software environment. The results verify effectiveness of the proposed electronic interface and the developed control system in regulating the generator output power while providing a high power quality at the microgrid.

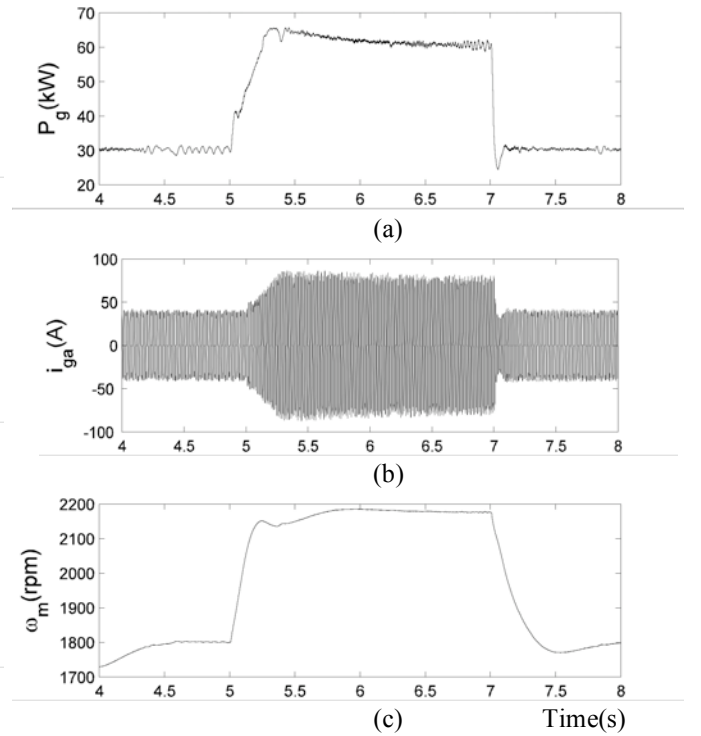


Fig. 14: Dynamic response of the synchronous generator of Fig. 8: (a) generator output power; (b) generator current; and (c) generator speed.

REFERENCES

- [1] P. Chiradeja and R. Ramakumar, "An approach to quantify the technical benefits of distributed generation," *IEEE Trans. on Energy Conversion*, Vol. 19, No. 4, pp. 764-773, December 2004.
- [2] L. F. Ochoa, A. Padilha-Feltrin, and G. P. Harrison, "Evaluating distributed generation impacts with a multi objective index," *IEEE Trans. on Power Delivery*, Vol. 21, No. 3, pp. 1452-1458, July 2006.
- [3] H. Nikkhajoei and M. R. Iravani, "A matrix converter based micro-turbine distributed generation system," *IEEE Trans. on Power Delivery*, Vol. 20, No. 3, pp. 2182-2192, July 2005.
- [4] G. Simons, P. Sethi, R. Davis, K. DeGroat, D. Comwell, and B. Jenkins, "The role of renewable distributed generation in California's electricity system," *IEEE PES Summer Meeting*, Vol. 1, pp. 546-547, July 2001.
- [5] R. C. Dugan and S. K. Price, "Issues for distributed generation in the US," *IEEE PES Winter Meeting*, Vol. 1, pp. 121-126, January 2002.
- [6] R. H. Lasseter and P. Piagi, "Control and design of microgrid components," *PSERC Publication 06-03*, University of Wisconsin-Madison, January 2006.
- [7] H. Nikkhajoei and R. H. Lasseter, "Microgrid protection," *IEEE PES General Meeting*, June 2007.
- [8] P. Piagi, "Microgrid control," Ph.D. dissertation, University of Wisconsin-Madison, 2005.
- [9] P. Piagi and R. H. Lasseter, "Autonomous control of microgrids," *IEEE PES Meeting*, Montreal, June 2006. http://certs.lbl.gov/CERTS_P_DER.html
- [10] R. H. Lasseter, A. Akhil, C. Marnay, J. Stephens, J. Dagle, R. Guttromson, A. Meliopoulous, R. Yinger, and J. Eto, "The CERTS Microgrid Concept," White paper for Transmission Reliability Program, Office of Power Technologies, U.S. Department of Energy, April 2002.
- [11] R. H. Lasseter, "MicroGrids," *IEEE PES Winter Meeting*, January 2002.
- [12] P. F. Ribeiro, B. K. Johnson, M. L. Crow, A. Arsoy, and Y. Liu, "Energy storage systems for advanced power applications," *IEEE Proceedings*, Vol. 89, No. 12, pp. 1744-1756, December 2001.
- [13] IEEE-SA Standards Board, "IEEE recommended practice for sizing nickel-cadmium batteries for stationary applications," *IEEE Standard 1115-2000*, March 2000.
- [14] N. Watson and M. S. Janota, "Turbocharging the internal combustion engine," *The Macmillan Press*, 1982.

- [15] S. Roy, O. P. Malik, and G. S. Hope, "Adaptive control of speed and equivalence ratio dynamics of a diesel driven power-plant," *IEEE Trans. on Energy Conversion*, Vol. 8, No. 1, pp. 13-19, March 1993.
- [16] J. A. Cook and B. K. Powell, "Modeling of an internal combustion engine for control analysis," *IEEE Control Systems Magazine*, Vol. 8, No. 4, pp. 20-26, August 1988.

Hassan Nikkhajoei (M05) received the B.Sc. and M.Sc. degrees from Isfahan University of Technology, Iran, and the Ph.D. degree from the University of Toronto in 2004, all in electrical engineering. He is currently a Research Associate at the University of Wisconsin-Madison. He was a postdoctoral fellow at the University of Toronto from 2004 to 2005, and a faculty member in Isfahan University of Technology from 1995 to 1997. His research interests include distributed generation power systems, power electronics, and electric machinery.

Robert H. Lasseter (F92) received the Ph.D. in Physics from the University of Pennsylvania, Philadelphia in 1971. He was a Consulting Engineer at General Electric Co. until he joined the University of Wisconsin-Madison in 1980. His research interests focus on the application of power electronics to utility systems and technical issues which arise from the restructuring of the power utility system. This work includes microgrids, control of power systems through FACTS controllers, use of power electronics in distribution systems and harmonic interactions in power electronic circuits. Professor Lasseter is a Fellow of IEEE, chair of IEEE Working Group on Distributed Resources: Modeling and Analysis, and an expert advisor to CIGRE SC14.